

# A Superficial Sulfur Interfacial Control Strategy for Fabrication of Sulfur/Carbon Composite for Potassium-Sulfur Batteries

Lei Hu<sup>a\*</sup>, Xianghe Meng<sup>a</sup>, Lingli Liu<sup>a</sup>, Dewei Liang<sup>a</sup>, Sheng Liang<sup>a</sup>, Li-Li Wang<sup>a\*</sup>, Lei Yang<sup>a</sup>, Tao Ding<sup>b</sup>, Chonghai Deng<sup>a</sup>, Qiang Dong<sup>a</sup>

a. School of Energy, Materials and Chemical Engineering, Hefei University, Hefei 230601, P. R. China.

b. National Synchrotron Radiation Laboratory, University of Science and Technology of China, Hefei, Anhui, 230029, PR China

## Experimental section

### Reagents

Tripotassium citrate monohydrate ( $C_6H_5K_3O_7 \cdot H_2O$ ), hydrochloric acid (HCl, 36.0~38.0 wt %), sublimed sulfur ( $S_8$ , >99.5 wt%), dichloromethane ( $CH_2Cl_2$ , >99.5 wt%) and ethanol were purchased from Shanghai Chemical Ltd. All chemicals are of analytical grade and were used without further purification.

**Preparation of microporous carbon.** The porous carbon was prepared using analogous synthetic methods previously. In a typical synthesis procedure, a certain amount of potassium citrate was placed in the corundum crucible, and react at a temperature of 750°C for 2.5 hours in a tube furnace under Ar atmosphere. Then, the obtained sample was washed three times with hydrochloric acid and water alternately. Finally, the obtained carbon material was collected and dried in a vacuum oven at 80 °C.

**Synthesis of S/C composite.** The resulting carbon was mixed with bulk sulfur (3:7 in a weight ratio) and sealed in a glass tube under vacuum. The glass tube was heated in a furnace at 155 °C for 10 h. To eliminate superficial sulfur, 0.5 g of the composite was washed by 15 ml of ethanol solvent for 5 min. Finally, the sample was labeled EA. In addition to ethanol, other extraction solvents (15 ml) such as ethanol/dichloromethane (2:1), ethanol/dichloromethane (1:2) and dichloromethane were also used to removing superficial sulfur. These sample were denoted as EAMC21, EAMC12 and MC, respectively.

**Characterizations.** X-ray diffraction (XRD) patterns were examined by X-ray powder diffractometry (Smart Lab, Rigaku, Japan) with Cu  $K\alpha$  radiation ( $\lambda = 0.15406$  nm). Nitrogen sorption isotherms and Brunauer–Emmett–Teller (BET) surface were conducted at 77K using a Micromeritics ASAP 2020 plus. The content of S was calculated by thermogravimetric analysis (TGA) in  $N_2$  atmosphere. The cycled cells were disassembled in an Ar-filled glove box, and the S cathodes were washed three times with DMC. The morphologies of cycled S electrode were observed by SEM

(Hitachi, SU8060, Japan). The composition information of the electrode was obtained using Thermo ESCALAB 250XI. The morphology structure of the S/C composites were analyzed by scanning electron microscopy (SEM). The structure of cathode was investigated using JEOL 2010F operated at 200 kV.

**Electrochemical measurements.** Firstly, the S/C Composite, Super P and PVDF binder dispersed in N-methylpyrrolidone (NMP) were uniformly mixing, at a weight ratio of 70: 20 : 10. The mixture was ball milled at 300 rpm for 3 hours. Then, the formed slurry was coated on Al foil by a doctor blade (gap : 300  $\mu\text{m}$ ) and dried at 110 $^{\circ}\text{C}$  for 10 h in a vacuum oven. The loading of active materials was 1.5–2.0  $\text{mg cm}^{-2}$ . potassium metal acted as a counter electrode. The electrolyte used for testing was 0.8 M  $\text{KPF}_6$  in 1 : 1 EC/DEC and the separator was whatman GF/D 1823. The cells were assembled in an argon-filled glove with the density of water and  $\text{O}_2$  all below 1 ppm and then aged for 12 h before testing to guarantee full access of the electrolyte with the electrode. Galvanostatic discharge–charge experiments were conducted on a battery-testing system (Land-CT2001A) in the potential range of 0.5–3 V (versus  $\text{Li/Li}^+$ ) at designated C-rates at room temperature (1C = 1675  $\text{mA g}^{-1}$ ). Cyclic voltammetry (CV) was performed using a CHI660D electrochemical workstation. Electrochemical impedance spectroscopy (EIS) were collected by an electrochemical workstation (Zahner Zennium Pro, Germany) with an AC amplitude of 5 mV in the frequency range of 10 kHz to 1Hz. The equivalent circuits and the data were fitted by using Nova software.

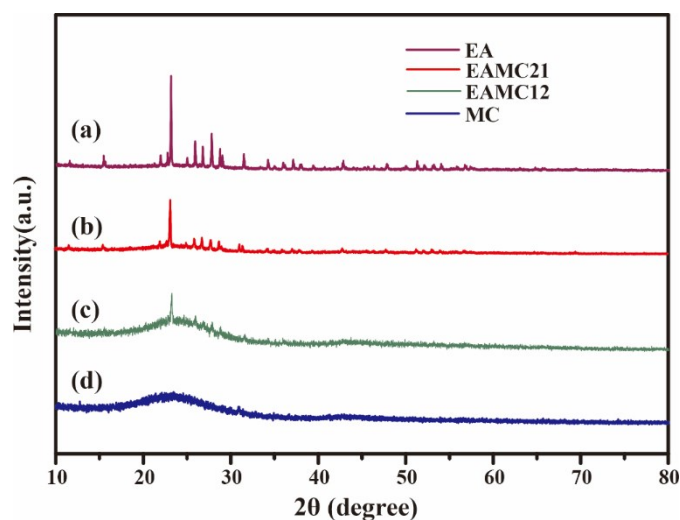


**Figure S1.** X-ray powder diffraction (XRD) patterns of (a) S/C composite washed with ethanol (EA); (b) S/C composite washed with ethanol/dichloromethane (2:1) (EAMC21); (c) S/C composite washed with ethanol/dichloromethane (1:2) (EAMC12); (d) S/C Composite washed with dichloromethane (MC);

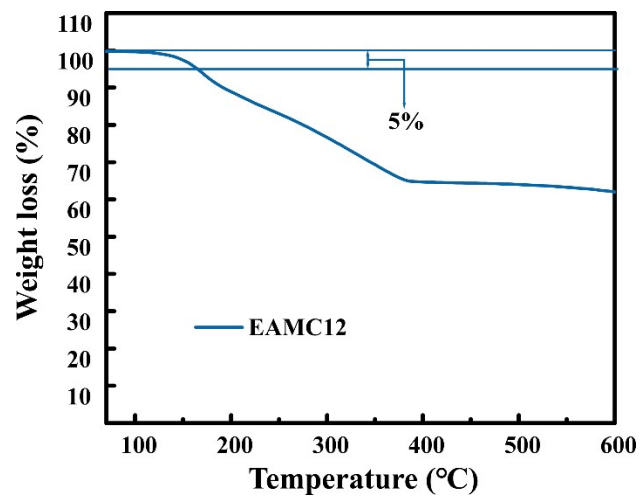


Figure S3. TGA curve of EAMC12 under N<sub>2</sub> atmosphere.

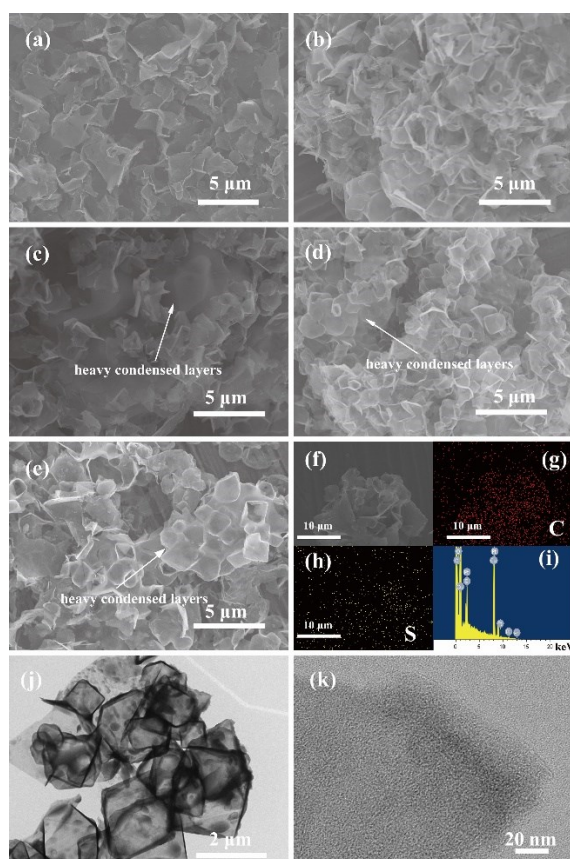
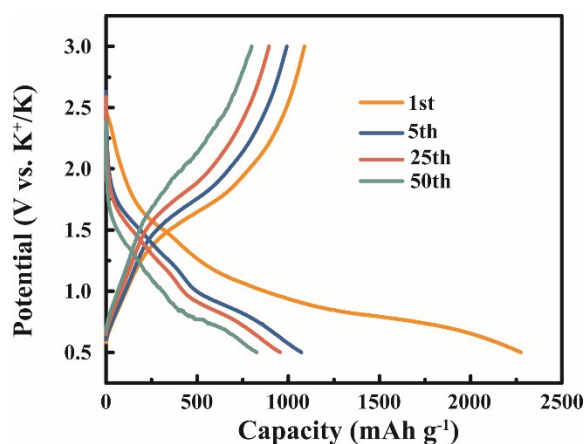
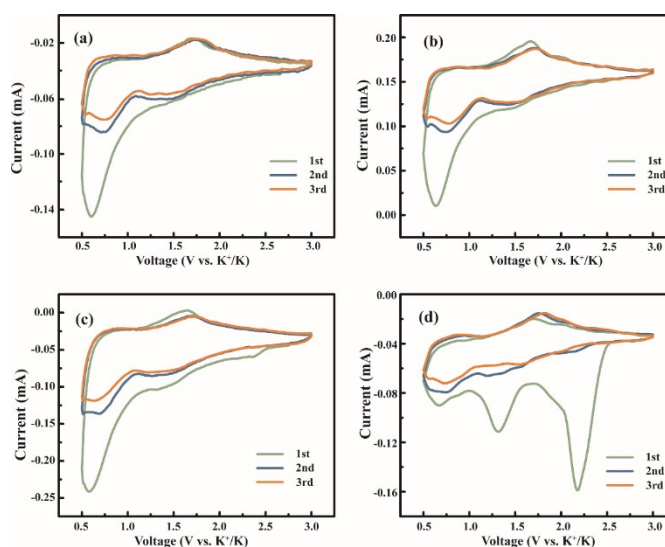


Figure S3. SEM images of (a)porous carbon; (b) MC; (c) EAMC12; (d) EAMC21; (e) EA; (f-i) the corresponding mapping data of EAMC21; (j) TEM images of EAMC12 and (k) HRTEM images of EAMC12.

In the scanning electron microscopy (SEM) image of **Figure S3a** exhibits the interlaced flake structure of porous carbon. The flake structure has a diameter of 2-3  $\mu\text{m}$  and a thickness of tens of nanometers. Compared with MC (**Figure S3b**), The SEM images (**Figure S3c**) clearly reveal EAMC12 present a rougher surface, implying that the surface may contain a small amount of sulfur. With the increase of ethanol content in washing agent, a more obvious heavy condensed layer appears outside the final products, which indicates that there is a large amount of sulfur on the outside of the carbon material (**Figure S3d** and **Figure S3e**). Elemental mapping of EAMC21 presents a uniform distribution of sulfur (**Figure S3f-i**). The Energy dispersive spectroscopy (EDS) mapping images taken from the region shows that sulfur is well dispersed in the porous carbon. TEM images (**Figure S3j**) further reveals a relatively thin layer structure, the high-resolution transmission electron microscopy (HRTEM) images(**Figure S3k**) confirm no apparent lattice fringe, suggesting a homogenous distribution of sulfur.



**Figure S4.** the charge-discharge curves of EAMC12 cathode at 0.2 C for various cycles.



**Figure S5.** cyclic voltammograms of at a scan rate of  $0.1 \text{ mV s}^{-1}$  between 0.5 and 3 V (a) MC cathode; (b) EAMC12 cathode; (c) EAMC21 cathode; (d) EA cathode;

The electrochemical behaviors of the cells were tested by using cyclic voltammograms (CV) from 0.5 to 3 V at 0.1 mV s<sup>-1</sup>. (Supporting information). **Figure S4a** provides the CV curves of MC cathode, which is identical to the discharge–charge curve. During the first discharge process, one obvious reduction peak is observed at 0.6 V vs. K<sup>+</sup>/K, while two cathodic peaks exist in successive cycles at about 1.55 V and 0.75 V, respectively, possibly demonstrating stepped reduction reaction between K ions and sulfur molecule.<sup>1</sup> By contrast, EAMC12 cathode (**Figure S4b**) presents a similar redox profile. As the sulfur content of the sample increases, an additional peak will appear around 2.3 V, which forms SEI films and indicates the irreversible reaction between sulfur molecule on the outer surface and ester molecules in electrolyte (**Figure S4c**).<sup>2</sup> For the case of EA(**Figure S3d**), the surface sulfur was not removed, there is a serious irreversible reaction in the first cycle. Hence, we proved that formation of the SEI film is mainly controlled by the amount of superficial sulfur.

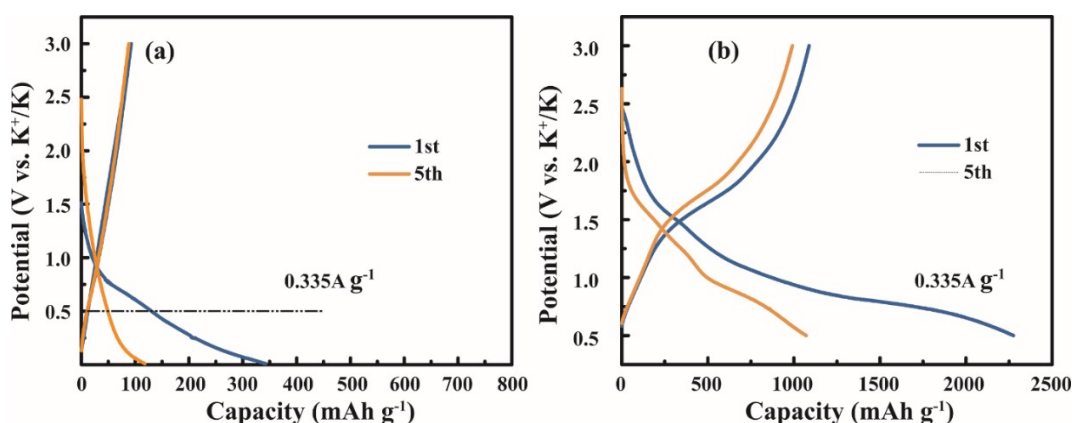


**Figure S6.** (a) Galvanostatic discharge/charge profiles of porous carbon in the 1st and 5th cycles; (b) the discharge-charge curves of EAMC21 in the 1st and 5th cycles;

The results (**Figure S6**) suggest that the first discharge capacity of porous carbon at current density of 0.335 A g<sup>-1</sup> is 341.9 mA h g<sup>-1</sup> (>0.01 V), while only 49 mA h g<sup>-1</sup> (> 0.5 V) remains after the 5th charging. Therefore, porous carbon contributes little to capacity in the voltage range of 0.5-3 V.

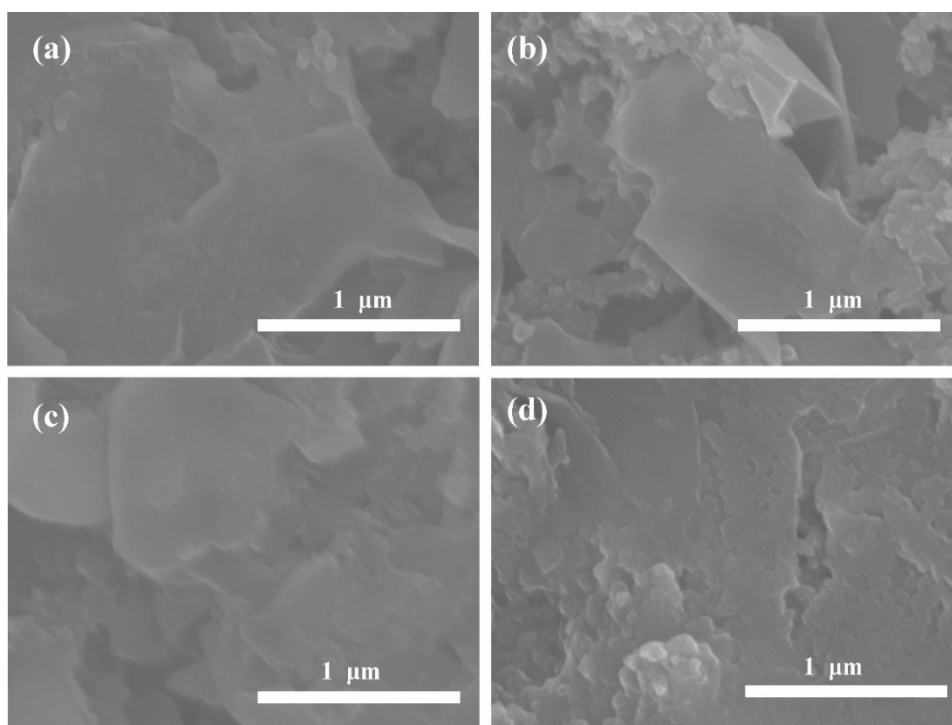


**Figure S7.** Morphologies of the microporous C/S composite electrodes after 1st cycle: (a) MC; (b) EAMC12; (c) EAMC21; (d) EA

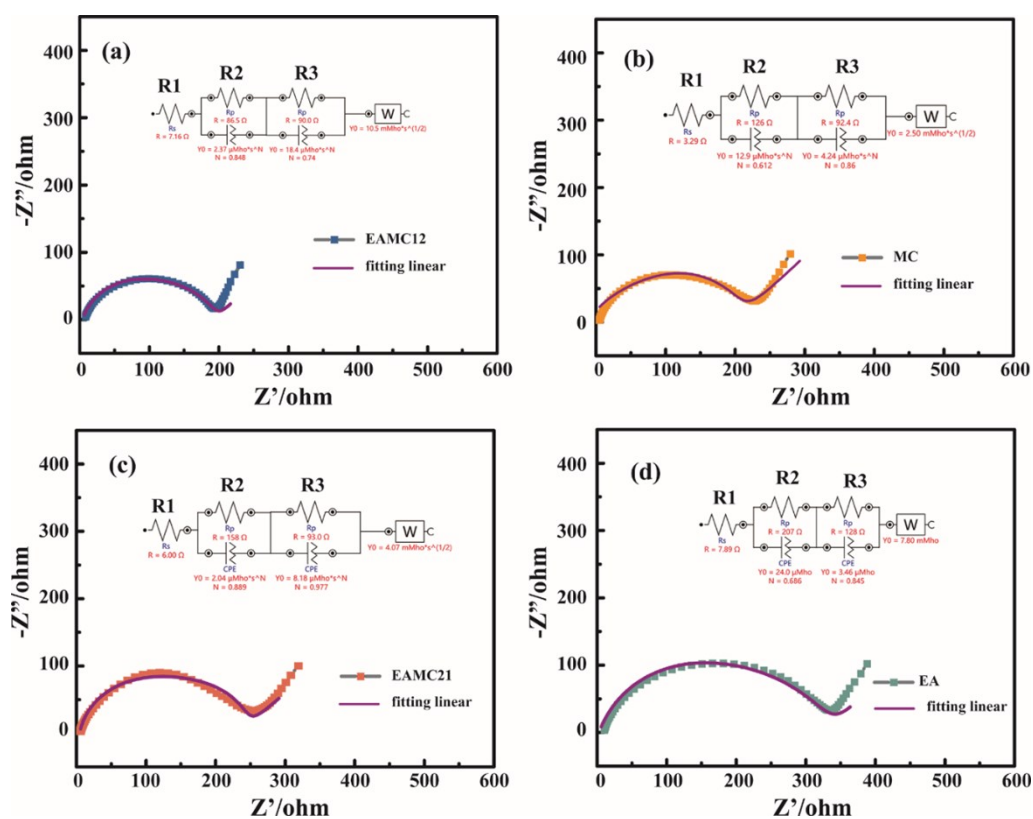


**Figure S8.** Nyquist plots obtained for the C/S electrodes after first cycle (a) EAMC12; (b) MC; (c) EAMC21; (d) EA (inset: equivalent circuits used to model the impedance spectra)

**Table S1.** Resistance obtained from the equivalent circuit fitting of experimental data

<b>Electrode</b>	<b>R<sub>1</sub></b>	<b>R<sub>2</sub></b>	<b>R<sub>3</sub></b>
<b>EAMC12</b>	7.2 $\Omega$	86.5	90 $\Omega$
<b>MC</b>	3.3 $\Omega$	126.0	92.4
<b>EAMC21</b>	6 $\Omega$	158.0	93 $\Omega$
<b>EA</b>	7.9 $\Omega$	207.0	128 $\Omega$

The morphology of the cycled microporous C/S composite electrodes was examined by SEM. In the case of MC, a relatively smooth surface was observed without any kinds of particle aggregation. For EAMC21 and EAMC12, the surfaces are slightly smooth without obvious agglomeration. As the sulfur content increases, the sulfur on the outer surface gradually reacts with the electrolyte, resulting in a thick stack layer and making the surface barely visible, which match well with XPS results (**Figure S7**). Electrochemical impedance spectroscopy was carried out on cycled microporous C/S composite electrodes to understand the interfacial charge. Semicircle in the high-frequency (HF) region is regarded as solid film resistance and the semicircle in the middle-frequency (MF) range is related to the charge-transfer resistance. The equivalent circuits for the impedance data are presented in **Figure S8**. According to the fitting results (**Table S1**), The R<sub>1</sub> corresponds to the resistance of the electrolyte. R<sub>2</sub>//CPE1 interpreted as an interphase contact resistance and its related capacitance in the sulfur electrode. R<sub>3</sub>//CPE2 is the charge transfer resistance and its related capacitance. The sloped line at the low frequency region can be related to Warburg impedance (Z<sub>w</sub>). For these four samples, The R<sub>1</sub> values are similar, demonstrating that these electrodes exhibit similar electrolyte resistance. Compared these three samples, EAMC21 has smallest the interphase contact resistance, Meantime, EAMC21 possess an obviously lower surface charge transfer (90  $\Omega$ ) resistance, indicating a much faster mass transport. The consequences of electrochemical impedance spectroscopy (EIS) match the electrochemistry performance well.

**Table S2.** Comparison of potassium-sulfur cell references and their electrochemical performances.

Cathode Composition	Electrolyte	Rate	Capacity (mA h g <sup>-1</sup> )	Cycles	S content (%)	Reference
S/CNF	KCF <sub>3</sub> SO <sub>3</sub> in TEGDME	0.2C	600	50	50 %	3
S/CMK-3	KTFSI in DEGDME (KNO <sub>3</sub> )	20mA g <sup>-1</sup>	283	10	76 %	4
PANI@S/CMK-3	KClO <sub>4</sub> in TEGDME	50mA g <sup>-1</sup>	329.3	50	40.8 %	5
PCNF/S	KFSI in DME	20 mA g <sup>-1</sup>	1380	250	25 %	6
<b>Carbon nanotube/ sulfur composites</b>	KFSI in DME	50mA g <sup>-1</sup>	180	5	70 %	7
SPAN	KPF <sub>6</sub> in EC/DEC	0.5 C	1050	100	45.5 %	8
SPAN	KPF <sub>6</sub> in EC/DEC	0.5 C	387	100	38 %	9
SPAN	KSO <sub>3</sub> CF <sub>3</sub> in EC/DEC	150mA g <sup>-1</sup>	253	300	39.25%	10
<b>Iodine-doping SPAN</b>	KPF <sub>6</sub> in EC/DEC	0.1 C	722	100	17.7 %	11
SPAN	KPF <sub>6</sub> in ED:DEC:DMC	35 mA g <sup>-1</sup>	490	100	39.52%	12
S/C composite	KPF <sub>6</sub> in EC/DEC	20mA g <sup>-1</sup>	869.9	150	20 %	1
<b>This work</b>	<b>KFP<sub>6</sub> in EC/DEC</b>	<b>0.2 C</b> <b>1C</b>	<b>826</b> <b>281</b>	<b>50</b> <b>500</b>	<b>37.8%</b>	

**References:**

1. P. Xiong, X. Han, X. Zhao, P. Bai, Y. Liu, J. Sun and Y. Xu, *ACS Nano*, 2019, **13**, 2536-2543.
2. S. Niu, G. Zhou, W. Lv, H. Shi, C. Luo, Y. He, B. Li, Q.-H. Yang and F. Kang, *Carbon*, 2016, **109**, 1-6.
3. X. Yu and A. Manthiram, *Energy Storage Materials*, 2018, **15**, 368-373.
4. L. Wang, J. Bao, Q. Liu and C.-F. Sun, *Energy Storage Materials*, 2019, **18**, 470-475.
5. Q. Zhao, Y. Hu, K. Zhang and J. Chen, *Inorg Chem*, 2014, **53**, 9000-9005.
6. X. Zhao, Y. Hong, M. Cheng, S. Wang, L. Zheng, J. Wang and Y. Xu, *Journal of Materials Chemistry A*, 2020, **8**, 10875-10884.
7. S. Gu, N. Xiao, F. Wu, Y. Bai, C. Wu and Y. Wu, *ACS Energy Letters*, 2018, **3**, 2858-2864.
8. J.-Y. Hwang, H. M. Kim and Y.-K. Sun, *Journal of Materials Chemistry A*, 2018, **6**, 14587-14593.
9. Y. Liu, W. Wang, J. Wang, Y. Zhang, Y. Zhu, Y. Chen, L. Fu and Y. Wu, *Chem Commun (Camb)*, 2018, **54**, 2288-2291.

10. R. Ma, L. Fan, J. Wang and B. Lu, *Electrochimica Acta*, 2019, **293**, 191-198.
11. S. Ma, P. Zuo, H. Zhang, Z. Yu, C. Cui, M. He and G. Yin, *Chem Commun (Camb)*, 2019, **55**, 5267-5270.
12. Y. Zhang, J. Lou, Y. Shuai, K. Chen, X. He, Y. Wang, N. Li, Z. Zhang and F. Gan, *Materials Letters*, 2019, **242**, 5-8.